# Experimental Investigation of Oblique Impact Behavior of Adhesively Bonded Composite Single-Lap Joints

M. Gokhan Atahan[1] 🔵 · M. Kemal Apalak[2]

## Abstract

Determining the impact behavior of adhesive joints allows the designing of high-strength joints. Therefore, the dynamic behavior of adhesive joints has recently become a trending research topic. The study aims to examine the impact behavior and damage mechanism of the adhesively bonded composite joints, taking into account different impact angles. The mechanical behavior of adhesively bonded glass-fiber reinforced laminated composite single-lap joints under bending impact load was experimentally determined via a drop weight impact test machine. The effects of impact angle ($\theta = 0°, 10°, 20°, 30°$), fiber angle ($\phi = 0°, 45°, 90°$), and overlap length ($b = 25, 40$ mm) on the impact behavior of the joints were investigated. These parameters were determined to affect the impact behavior of the joint and the damage characterization. The highest contact force occurred in the joints with 0° fiber angle having the highest bending strength, and the lowest contact force occurred in the joints with 90° fiber angle having the lowest bending strength. Due to the increase in the impact angle, the maximum contact force value in the joints decreased, while the total contact time increased. The increase in overlap length had little effect on the maximum contact force and total contact time, and the vertical displacement decreased due to the increasing bending stiffness. The unbalanced joint with 45° fiber angle was forced to rotate around its axis due to in-plane unbalanced shear stress distributions induced by the bending impact load. The unbalanced shear stress distribution caused shear damage at the fiber-matrix interface and the top composite-adhesive interfaces. In joints with 0° fiber angle, the impact energy was mostly met with adhesive damage, while the composite adherend was damaged as a result of increased shear stresses in the matrix region for the joints with 90° fiber angle.

---

✉ M. Gokhan Atahan
  gatahan@erciyes.edu.tr

1   Department of Mechanical Engineering, Abdullah Gul University, Kayseri, Turkey

2   Department of Mechanical Engineering, Erciyes University, Kayseri 38039, Turkey

# 1 Introduction

Although there are many classical joining methods, such as welding, riveting and bolting, the adhesive bonding method has widespread usage in industrial areas because it offers many benefits. Since it provides uniform stress distribution throughout the bonding region, it contributes positively to the fatigue strength of the joints. In addition, other benefits of adhesive joints are that they are lightweight, relatively easy to apply compared to other joining methods, damage can be detected at an early stage before they are completely separated, and it is possible to take precautions [1–3]. Adhesive joints may exhibit different mechanical behavior due to the strain rate effect under impact load from their behavior under quasi-static load [4]. Harris and Adams [5] determined the impact strength and energy absorption capacity of adhesively bonded single-lap joints for four different epoxy adhesives and three aluminum alloy adherends. They determined that the increase in the plastic deformation ability of the adherends increased the energy absorption capacity of the joint. Srivastava et al. [6] developed an experimental method with a novel specimen geometry to determine the dynamic shear strength of adhesively bonded single-lap joints. They showed that the dynamic shear strength of the joint was greater than its static shear strength. Yokoyama [7] investigated the tensile strength and energy absorption ability of adhesively bonded butt joints under dynamic load. They reported that the joint tensile strength increased significantly with increasing loading rate and was importantly affected by the adhesive layer thickness and the mechanical properties of the adherend material. In addition to the experimental study, the finite element analysis method has been preferred by many researchers to predict the impact behavior of adhesively bonded joints [8–14].

The adhesive bonding method is particularly useful for joining composite materials. As a result of the improvement in the mechanical properties of adhesives, the adhesive bonding method provides a reliable structure in many areas, such as the automotive, defense, aviation, and marine industrial sectors [1–4, 15]. Adhesively bonded composite joints are widely used in industrial sectors where lightweight structures are preferred. The determination of the behavior of these joints under dynamic loads is necessary for the design of similar and dissimilar joints. For this reason, many researchers have studied the behavior of adhesively bonded composite joints under dynamic load [16]. Chen et al. [17] studied the behavior of thermoplastic single-lap double rivet joints with and without adhesive under out-of-plane projectile impact and quasi-static concentrated loads. Bautista et al. [18] investigated the dynamic response of glass fiber reinforced composite single-lap joint used in military aircraft. Araújo et al. [19] determined the impact behavior of adhesively bonded composite single-lap joints used in the automotive industry. Hou et al. [20] analysed the failure characteristics of twill-woven carbon fiber reinforced thermoplastic tubular T-joints under impact load. Machado et al. [21] studied the effect of temperature and overlap length on the mechanical behavior of adhesively bonded composite single-lap joints under quasi-static and impact loads. Basri et al. [22] investigated the dynamic characteristics of adhesively bonded carbon fiber reinforced composite structure.

Adhesively bonded joints are expected to exhibit the best performance, especially under impact load. This expectation has led many researchers and engineers to determine joint behavior under dynamic loading. Determining the mechanical behavior of materials and joints under impact load requires complex mathematical modelling and analysis, advanced experimental testing equipment, and new analysis methods of experimental results. The use of high-performance sensors and data acquisition equipment to obtain impact test data leads to the provision of a suitable experimental laboratory environment at high costs.

Determining the mechanical properties of an adhesive joint under static and dynamic loads makes it possible to design a high-strength joint under impact load. Commonly used joint types in the study of impact behavior are: single-lap joint, double-lap joint, butt-joint, rod-ring joint, and hat shaped joint. Advances in composite material design have led to the need to combine the parts manufactured from composite material in industrial applications. Adhesively bonded composite joints provide high mechanical strength as well as lightness and ease of application. The main reason for preferring the use of adhesives for joining composite materials is that the use of rivets and screws requires holes causing local stress concentrations in the composite material between holes and weakening the strength of the joint [4]. Studies in the literature on the determination of the impact behavior of joints generally examined the effect of impact load in the perpendicular direction to the joint [23–29].

Kadioglu and Adams [30] studied the behavior of flexible adhesively bonded single-lap joints under low velocity impact. They also performed quasi-static loading test to determine the effect of loading rate on the joint strength. They found a significant increase in the joint strength under the impact load compared to the quasi-static load strength. They revealed that there is a relationship between the joint strength and loading rate. Hazimeh et al. [31] investigated the effect of fiber angle on peel and shear stress in the adhesively bonded composite double-lap joints under impact load. They showed that the stress variation in the adhesive was not affected by the fiber angle direction for the longitudinal direction. However, they determined that the highest stress in the adhesive occurred when the fibers were placed along the loading direction [0°], while the lowest stress occurred when the fibers were placed perpendicular to the loading direction [90°]. In addition, it was reported that the stress in the adhesive increased with the increase in the longitudinal stiffness of the composite materials. Atahan and Apalak [32] investigated the behavior of adhesively bonded single lap joints under low velocity bending impact load. The effect of the plastic deformation capabilities of the adherend materials on the adhesive damage mechanism and the effect of the overlap length and impact energy on joint behavior under impact load were determined. The damage initiation and propagation of adhesive were investigated by determining the damaged residual adhesive thicknesses on the overlap surfaces with the SEM images. Liu and Yan [33] applied impact energy (4 to 30 J) at five different points in the bonding region to detect the impact load-sensitive region of composite patch repair joint. Thus, the effect of impact load variation on adhesive damage was investigated. After the impact tests, they also applied a tensile test to determine the load carrying capacity of the joints and the impact energy threshold level for the joints was found to be 23 J. Only the composite material was damaged at low impact energy, while damage occurred in both the composite adherend and the adhesive at high impact energy levels. Huang et al. [34] investigated low-energy impact and post-impact fatigue damage of composite-steel and composite-composite adhesively bonded single-lap joints. They reported that the post-impact fatigue life increased as the flexural stiffness ratio between the adherends and the adhesive decreased. Silva et al. [35] studied impact response of an adhesively bonded automotive structure consisting of AA6016T4 substrates and XNR6852 E-3 adhesive. An early failure in the structures bonded with crash resistant epoxy adhesive occurred due to the presence of holes leading to high stress concentrations in the lower substrate. Li et al. [36] investigated cohesive failure, energy absorption, and post-load-bearing capacity of the adhesively bonded single-lap joints for four different temperatures and four different transverse impact energies. They reported that a V-shaped stress distribution occurred under the transverse impact load and the stress increased towards the free edges and since the stress was highest at the free edges, the crack initiated at the edge. The damage area and crack length increased with impact energy and

temperature increase. Machado et al. [37] predicted the behavior of dissimilar composite-aluminum adhesive joints under quasi-static and impact loads considering temperatures ranging from -30 to 80 °C. The results showed that, for the quasi-static condition, the aluminum-aluminum joints absorbed the most energy due to its high plastic deformation ability, whereas the CFRP-CFRP joints absorbed more energy because of frictional sliding during delamination under impact load. Avendaño et al. [38] determined the strength of dissimilar single-lap joints under quasi-static and impact loads considering different temperature. It was reported that the mechanical property of the adherends had a significant effect on the failure of single-lap joints. In addition, adherends and adhesive damage characteristics were affected by the test temperature. The review of the present studies indicates that the studies on the oblique impact effect are generally applied to certain materials and structures whilst studies on adhesive joints are very limited. Song [39] investigated the effects of load angle, window width and height, and impact velocity on the behavior of windowed tubes under oblique impact load. A new design method was proposed by aiming effectively increase the critical impact load angle of the tube without compromising the energy absorption capacity and it was reported that the energy absorption ability of the structure decreased as the cell height increased. Ivañez et al. [40] investigated the behavior of composite sandwich plates under low velocity oblique impact loads and the effect of impact angle and impact energy in terms of maximum contact force, total contact time, absorbed energy, maximum displacement of the impactor, and damage areas. They observed that as the contact area between the impactor and the sample decreased with the increase in the impact angle, the damage area of the sample decreased and the maximum contact force value and the amount of absorbed energy decreased with increasing impact angle.

Adhesive joints are used in many industrial areas where structural integrity is essential, such as aeronautics, aerospace, electronics, and automotive [2]. Various static and dynamic mechanical tests are used to determine the strength of adhesive joints. One of the dynamic mechanical tests is the low-speed impact test. The dynamic behavior of the adhesive joint obtained from the low-speed impact test is an essential source of information for industrial applications. Adhesive bonded joints may experience to quasi-static and dynamic loads in arbitrary directions in practice. Examining the mechanical behavior of adhesive joints under oblique impact load is expected to provide important information for the design of joints subjected to arbitrary impact loads. Many industrial areas, especially the automotive industry, prefer adhesive joints extensively to increase mechanical strength, reduce weight and simplify production. Since the automotive industry needs to provide an adequate safety level during vehicle collisions, engineers and researchers have focused on determining the impact behavior of adhesive joints. Mastering the behavior of adhesively bonded joints under impact load allows the design of stronger and safer structures [4]. In the literature, the mechanical behavior of the adhesive joints under out-of-plane impact was investigated by considering only the normal (transverse) impact load. However, the normal and shear stress components change depending on the impact angle, affecting the adherend and adhesive damage. Therefore, as well as the joint behavior under the normal impact, the mechanical behavior under oblique impact should be considered for adhesive joint design. The present study examines the impact behavior of composite joints by considering both normal and oblique impact loads, and the effect of oblique impact on joint damage in detail. In addition, it evaluates the effects of fiber orientation angle and overlap length, which are important design parameters for adhesively bonded composite joints, on the impact behavior and damage mechanism of the joints. Adhesive joints can be subjected to different oblique impact loads. Depending on the impact angle, different stress-strain states may occur in different regions of the adhesive joint, and the damage mechanism may

differ. Mastering the low velocity oblique impact behavior of adhesively bonded composite joints will be an important source of information for researchers and engineers working in this field. In this study, the effects of impact angle, fiber angle and overlap length on the impact behavior of adhesively bonded composite single-lap joints were experimentally investigated via a drop weight impact test machine.

## 2 Experiment and Method

Low speed impact tests were performed for different impact angles ($\theta = 0°$, 10°, 20°, 30°) and overlap lengths ($b = 25$ and 40 mm) to determine the bending impact behavior of glass fiber reinforced composite single-lap joints with different fiber angles ($\phi = 0°$, 45°, 90°). The main purpose of the experimental study was to compare the effects of variable parameters under oblique impact load with those of normal impact load. Determining the mechanical behavior of adhesively bonded composite single-lap joints for different impact angles is very important for high-strength joint design. The two orthogonal components of the bending impact load with varying impact angles will affect the distributions of the normal and shear stresses in the joint. As the impact angle increases, the bending moment and the peel stresses on the free edges of the overlap region decrease. In contrast, the shear stresses in this area increase and become more effective on the adhesive damage. Therefore, the mechanical behavior of the joint under normal and oblique impact loads was investigated with four different impact angles (0°, 10°, 20°, and 30°). Purimpat et al. [41] determined that the fiber orientation angle affected the composite joint behavior under quasi-static load. They stated that the joints with 0°, 45°, and 90° fiber angles are commonly used in industrial applications. In addition, to examine the effect of adherend strength on adhesive damage, the adherends with the highest (0° fiber angle) and lowest (90° fiber angle) strength were considered. These two different fiber angles were preferred to observe the mechanical behavior of the joint under impact load for the joints having the highest and lowest load carrying capacities. The fact that the top and bottom composite materials have 45° fiber angles in the same direction creates an unbalanced joint type. A joint type, unbalanced under bending impact load, has different damage types than the other two balanced joint types (0° and 90°). The unbalanced joint rotates under impact load, affecting the initiation and propagation mechanism of adhesive damage. For this reason, different fiber angles ($\phi = 0°$, 45°, and 90°) were preferred to examine the effect of composite fiber orientation angle on the behavior of the composite joint under dynamic load. It is sufficient to determine the effect of these selected critical fiber angles ($\phi = 0°$, 45°, and 90°) on the joint behavior and to compare the mechanical behavior of other fiber-angle designs. Another important parameter affecting the behavior of the adhesively bonded joints under dynamic load is the overlap length. Increasing the adhesive volume increases the joint stiffness. Machado et al. [21] investigated the effect of overlap length on the mechanical behavior of composite single-lap joints under quasi-static and in-plane impact loads. They indicated that the increase in overlap length increased the joint strength. In this study, the effect of overlap length on the out-of-plane impact behavior of the joint was investigated for two different overlap lengths (b = 25 and 40 mm). Preliminary tests were carried out to determine the impact load applied to the composite single-lap joints. After the preliminary tests, considering the integrity of the joints with the highest bending strength of 0° fiber angle, the impact velocity of v = 1.1 m/s corresponding to 3.2 J impact energy was found suitable for this study. Impact velocity was kept constant in all tests, and the effects of impact

angle, fiber orientation angle, and overlap length on the impact behavior of the joints were investigated.


## 2.1 Specimen Production

Glass fiber reinforced composite adherends were manufactured using the vacuum infusion method. The unidirectional glass-fiber with an area density of 600 g/m$^2$ and epoxy required to manufacture composite plates were obtained from Dost Chemical Industry in Turkey. In order to produce the composite material having good mechanical properties, air leaks that may occur during the vacuum process should be prevented as much as possible. For this purpose, dirt and residues that may damage the vacuum nylon were cleaned and the manufacturing process started. The manufacturing stages of the composite plate using vacuum assisted resin transfer molding (VARTM) process are shown in Fig. 1 are summarized as follows:

- First, the film layer was fixed using double-sided sealing tape, and four unidirectional glass fiber fabrics, each with an area density of 600 g/m$^2$, were placed on this film layer.
- The peeling fabric was placed on the fibers, in order to facilitate the peeling process of the vacuum nylon from the composite plate and to remove the air bubbles that might occur during the vacuum process.
- On the peeling fabric, infusion mesh was laid in order to ensure the flow of epoxy resin in the vacuum nylon and spiral infusion pipes, required for the vacuum process were placed (Fig. 1a).
- Before the epoxy was transferred to the vacuum bag, the air in the bag was vacuumed by means of the pump and air leakage was checked.
- After checking for air leaks, MGS L160 epoxy resin, with hardener, was pumped into the vacuum nylon (Fig. 1b).
- After the epoxy resin spread in the vacuum nylon and covered the entire area, air entry and exit of the vacuum bag were prevented.
- Finally, a homogeneous temperature distribution (120 °C) was applied on the composite plate for 1 h to ensure good curing.

At the end of the manufacturing process, a composite plate with an average thickness of 2 mm was obtained. The adhesively bonded composite joints were manufactured from
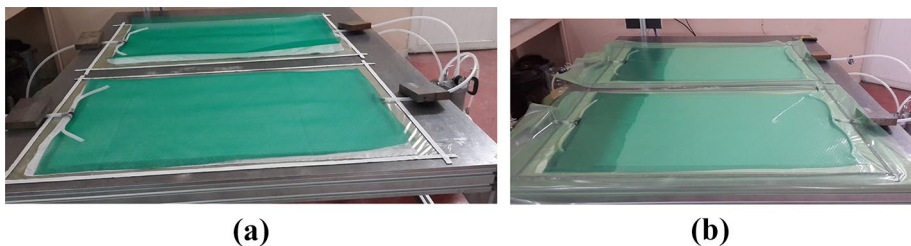


(a)                                   (b)

**Fig. 1** Manufacturing stages of glass fiber reinforced composite: (**a**) placing the infusion mesh, (**b**) impregnating the epoxy

two composite plates with a dimension of $100 \times 125$ cm; thus, composite adherends with dimensions of 112.5x25x2 and 120x25x2 mm were cut from these plates.

## 2.2 Mechanical Properties

The material properties of the composite adherend were determined by considering various test standards. Mechanical properties were determined according to the ASTM D3039-76 test standard [42] for tensile test, ASTM D3410-87 test standard [43] for compression test, and ASTM D7078-19 test standard [44] for shear test. At least five specimens were tested for each test. The images of the glass-fiber reinforced composite test specimens after the mechanical tests are presented in Fig. 2. The tensile strengths ($X^T$ and $Y^T$) and the elasticity modulus ($E_1$ and $E_2$) of the composite material were determined by the tensile test. The compression strengths of the composite material ($X^C$ and $Y^C$) were determined by the compression test. In addition, in-plane shear strength of the composite material was determined by the shear test. The in-plane shear modulus ($G_{12}$) was determined experimentally and transverse shear modulus ($G_{13}$) was assumed equal to the in-plane shear modulus ($G_{12}$)

**(a)** longitudinal tensile test

**(b)** transverse tensile test

**(c)** longitudinal compressive test

**(d)** transverse compressive test
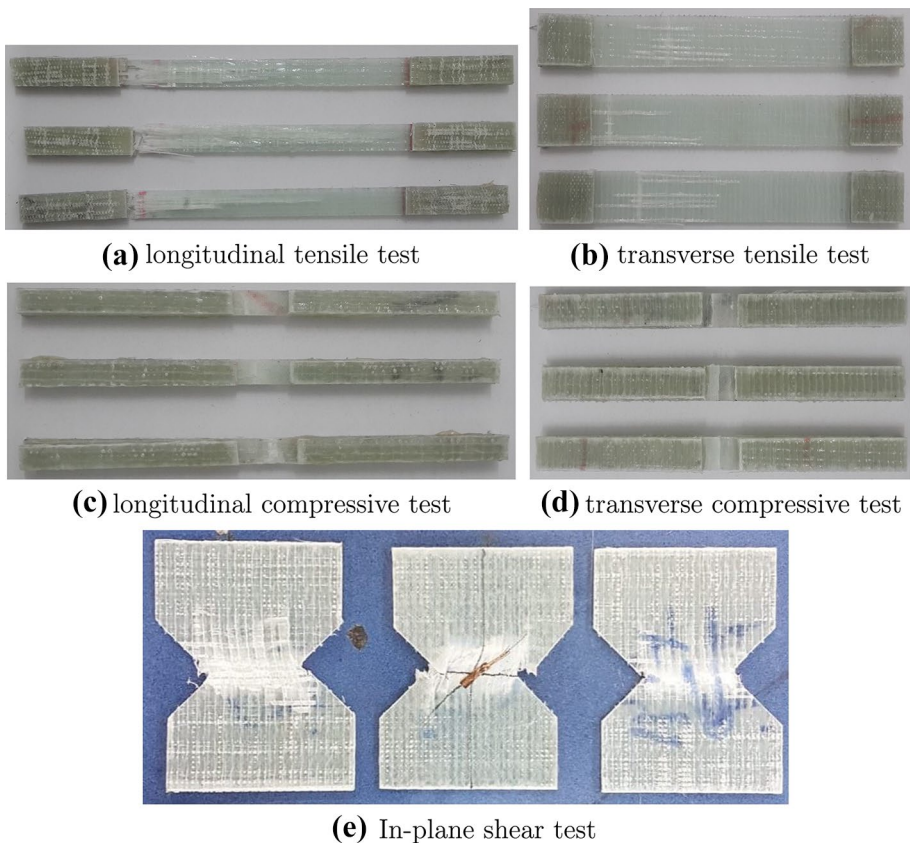
**(e)** In-plane shear test

**Fig. 2** The images of the glass fiber reinforced composite test specimens after the mechanical tests (**a**) longitudinal tensile test (**b**) transverse tensile test (**c**) longitudinal compressive test (**d**) transverse compressive test (**e**) In-plane shear test

for unidirectional fiber-reinforced lamina. The through-thickness shear modulus ($G_{23}$) was determined by following equation [45].

$$G_{23} = \frac{E_2}{2(1 + \upsilon_{23})} \tag{1}$$

Poisson's ratios ($\upsilon_{12}$, $\upsilon_{23}$) [45], interlaminar shear strength ($S_{23}$) [46, 47], and fracture toughnesses ($G_{ft}^c$, $G_{fc}^c$, $G_{mt}^c$, $G_{mc}^c$) [48] values of composite materials were obtained from studies in the literature. Table 1 shows the measured and already available mechanical properties of the glass fiber reinforced composite material.

## 2.3  Preparation of Composite Single-lap Joints

25 × 112.5 mm pieces for 25 mm overlap length and 25 × 120 mm pieces for 40 mm overlap length were cut from the composite plate in 2 mm thickness. Due to the manufacturing method, one of the composite material surfaces was rough and the other surface was relatively less rough and shiny. Adhesive was applied to the rough surfaces to achieve better adhesion strength. In order to remove dirt, dust, and other residues on the bonded surfaces, the surfaces were cleaned with ethanol before the bonding process. Araldite 2015 [49] adhesive was applied to the cleaned bonded surfaces and was spread homogeneously on the surface. The top and bottom apparatuses were used to provide the desired adhesive thickness in single-lap joints. Single-lap joints were placed between the top and bottom apparatuses (Fig. 3a). Four holes of 6 mm diameter in the corner regions of these apparatuses and four 4.2 mm thick washers were used to achieve a uniformly distributed adhesive layer in an adhesive thickness of 0.2 mm. Single-lap joints placed between the top and bottom apparatus were kept for curing at room temperature for 2 days (Fig. 3b).

Table 1  Mechanical properties of glass fiber reinforced composite material

| Property | Symbol | Unit | Value |
|---|---|---|---|
| Longitudinal modulus of elasticity | $E_1$ | GPa | 34.10 |
| Transverse modulus of elasticity | $E_2 = E_3$ | GPa | 10.30 |
| Shear modulus | $G_{12} = G_{13}$ | GPa | 3.60 |
| Shear modulus | $G_{23}$ | GPa | 3.68 |
| Poisson's ratio [45] | $\upsilon_{12} = \upsilon_{13}$ | | 0.278 |
| Poisson's ratio [45] | $\upsilon_{23}$ | | 0.40 |
| Density | $\rho$ | kg/m$^3$ | 1830 |
| Longitudinal tensile strength | $X^T$ | MPa | 750.50 |
| Transverse tensile strength | $Y^T$ | MPa | 62.80 |
| Longitudinal compressive strength | $X^C$ | MPa | 248.04 |
| Transverse compressive strength | $Y^C$ | MPa | 112.40 |
| In-plane shear strength | $S_{12} = S_{13}$ | MPa | 52.90 |
| Interlaminar shear strength [46, 47] | $S_{23}$ | MPa | 38 |
| Longitudinal tensile fracture energy [48] | $G_{ft}^c$ | N/m | 12,500 |
| Longitudinal compressive fracture energy [48] | $G_{fc}^c$ | N/m | 12,500 |
| Transverse tensile fracture energy [48] | $G_{mt}^c$ | N/m | 1000 |
| Transverse compressive fracture energy [48] | $G_{mc}^c$ | N/m | 1000 |
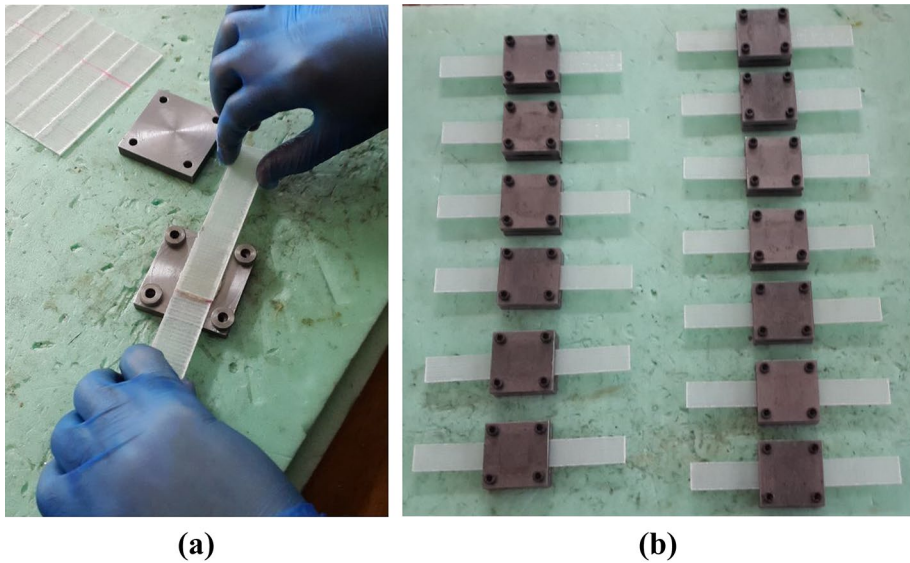
**Fig. 3** Preparation of composite single-lap joints: (**a**) placing the joint between apparatuses (**b**) holding between apparatuses during adhesive curing

## 2.4 Impact Test

Low speed impact tests of single-lap joints were carried out via the Fractovis Plus impact test machine. Four different impact angles ($\theta = 0°$, 10°, 20°, 30°) were considered in low speed impact tests. In order to fix the sample in the impact test, one apparatus was manufactured for each impact angle so that the joint can be fixed at the desired angle value, the impact load can be applied to the midpoint of the joint, and the distance between the holders ($L = 160$ mm) can remain the same in all tests. The Fractovis Plus impact test machine and specimen holding apparatus are shown in Fig. 4. The joint dimensions and impact test conditions in this study were determined according to the study performed by Vaidya et al. [50]. The main parts of the impact test machine: the impactor sensor with a capacity of approximately 40 kN that measures the contact force value generated during the test, the speed sensor that measures the speed of the impactor when the impact load is applied to the sample, and the anti-rebound system that prevents repeated impact to the sample. The single-lap joint dimensions used in the impact test are shown in Fig. 5. The effective length ($L = 160$ mm) was kept constant at all impact angles ($\theta = 0°$, 10°, 20°, 30°). The overlap length ($b$) was determined as 25 and 40 mm in order to examine the effect of the overlap length on the impact behavior. A semi-cylindrical impactor with a radius of 5 mm and a width of 25 mm was used in the impact test. The total mass of the impactor was 5.302 kg. Impact tests were carried out for an impact energy of $E = 3.2 \pm 0.16$ J. After each impact test, contact force–time and contact force–displacement graphs were prepared with the data obtained from the impact machine. The effects of test parameters (impact angle, fiber angle, and overlap length) on contact force–time and contact force–displacement were examined and discussed in detail in the following sections. In addition, damage initiation and propagation mechanisms were evaluated by examining the microscope images of adhesive damage surfaces.
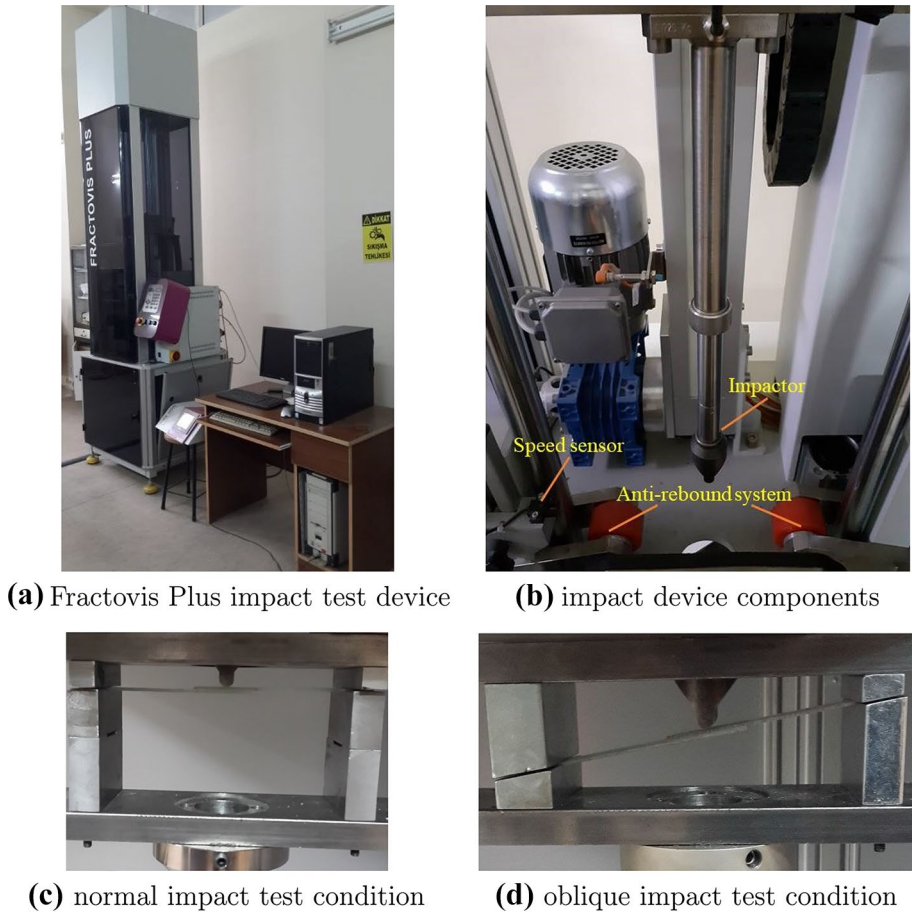
**(a)** Fractovis Plus impact test device



**(b)** impact device components



**(c)** normal impact test condition



**(d)** oblique impact test condition

**Fig. 4** Fractovis Plus impact test device and specimen holder apparatus (**a**) Fractovis Plus impact test device (**b**) impact device components (**c**) normal impact test condition (**d**) oblique impact test condition

## 3 Experimental Results

Low speed impact tests were carried out to examine the effect of variations in impact angle, fiber angle, and overlap length on the bending impact behavior of the single-lap joint. For this purpose, four different impact angles: $\theta = 0°$, $10°$, $20°$ and $30°$, three different fiber angles: $\phi = 0°$, $45°$ and $90°$, and two different overlap lengths: $b = 25$ and $40$ mm were considered in the experimental study. Impact energy ($E = 3.2 \pm 0.16$ J) was constant for all impact tests.

### 3.1 Effect of Impact Angle

Figure 6 shows the effect of the impact angle on the contact force–time variations. The increase in the impact angle decreases the contact force component of the impactor in the normal direction, while increasing the component in the tangential direction. Therefore, the
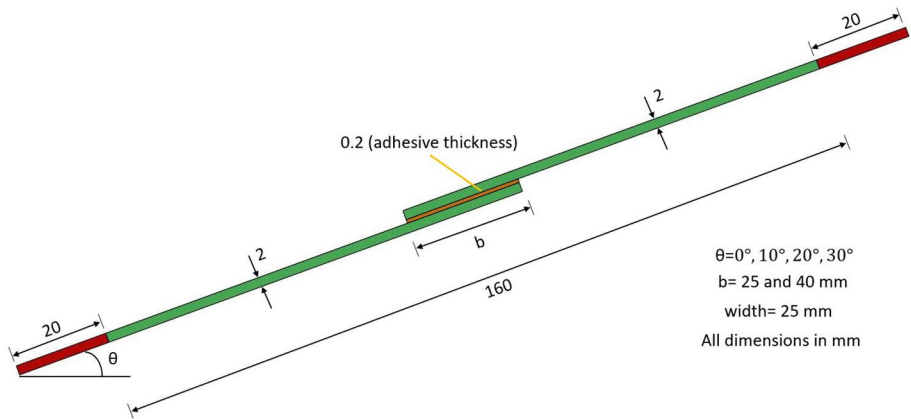
**Fig. 5** Dimensions of single-lap joint

contact force value decreases, the contact time increases as the lateral area of the impactor contacting the joint increases with the increase of the impact angle. Some amount of the impact energy that the impactor possesses after it encounters the joint is absorbed by the joint, the remaining energy is released as rebound energy. In order to prevent repeated impacts to the joint, the anti-rebound system is activated by the sensors and keeps the impactor up without contacting the sample. However, for large impact angles of 20° and 30°, the increase in the lateral contact surface becomes apparent and the rebound energy of the impactor decreases to very low levels, so the normal component of the contact force cannot reach zero value.

Similarly, in joints with an overlap length of 40 mm, the increase in the impact angle decreased the normal component of the contact force and increased the total contact time. The contact force–time curves were quite similar for the 20° and 30° impact angles. In joints with 45° fiber angle under impact load, rotation about the joint axis occurs due to the unbalanced joint type. Due to the rotation of the joint, the contact surface region between the impactor and the joint increases. The single-lap joints with 45° fiber angle for 30° impact angle had a longer total contact time than the single-lap joints with other fiber angles. In case the contact force–time variations of the joints under the normal impact (0°) are examined, the total contact time is approximately 50 ms in the single-lap joints with 0° fiber angle, while the total contact time is in 30–40 ms for 45° and 90° fiber angles. The single-lap joint with the highest bending strength exhibited the longest total contact time. In case the highest contact force values occurring in the single-lap joints with 25 mm overlap length were compared for 0°-30° impact angles; the maximum contact force decreased from 494.7 to 317.8 N in the single-lap joints with 0° fiber angle, the maximum contact force value decreased from 333.7 to 262 N in the single-lap joints with 45° fiber angle, and the highest contact force value occurred for 90° fiber angle and decreased from 356.6 to 172.8 N. With the increase in the impact angle, the decrease in the maximum contact force value in the joints was approximately 36, 21, and 52% for 0°, 45° and 90° fiber angles, respectively. For 40 mm overlap length, the rate of decrease in maximum contact force value for 0°, 45°, and 90° fiber angles was 21, 31, and 34%, respectively. As seen, the contact force was directly related to the bending strength of the joint. Namely, the increase in the impact angle and the decrease in the contact force was minimum in the joint with the highest bending strength with 0° fiber angle. The highest reduction in the contact force
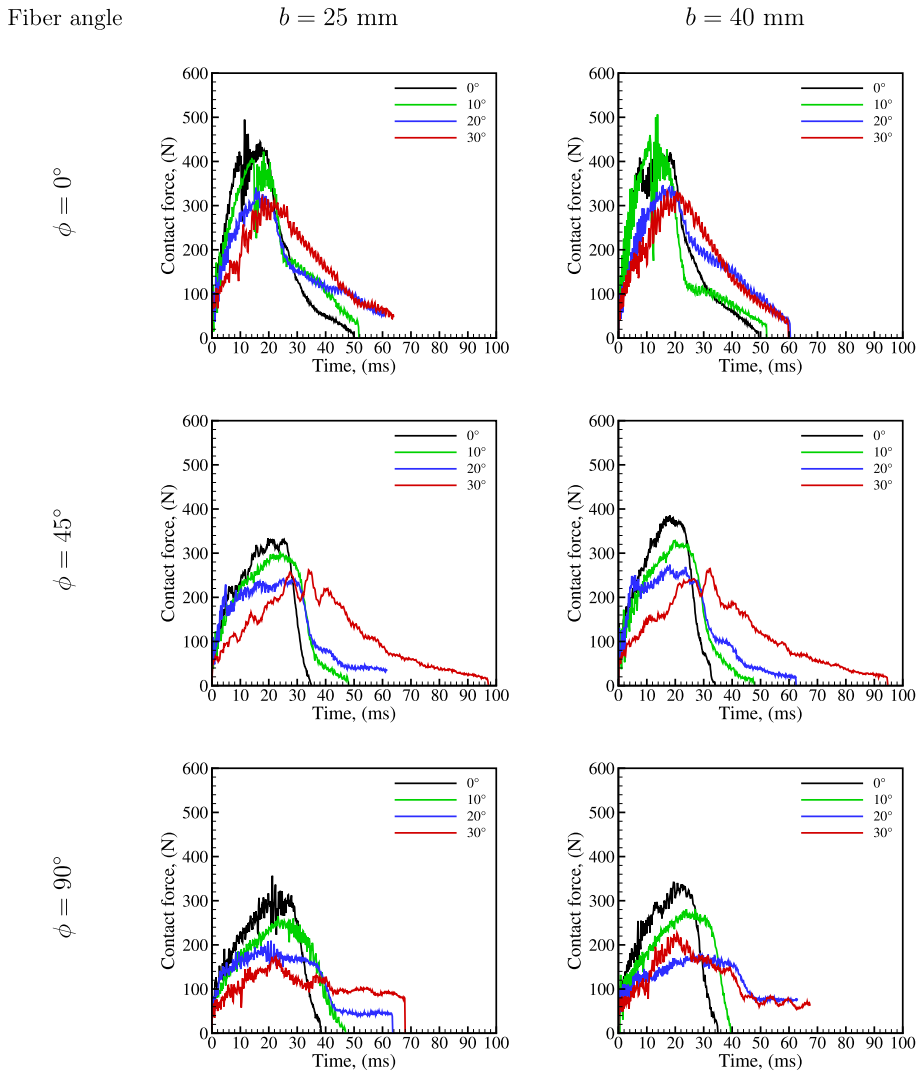
**Fig. 6** Contact force–time variations of composite single-lap joints under different impact angles (*b*: overlap length, $\phi$: fiber angle)

level was observed in the joint having 90° fiber angle with the lowest bending strength. In this type of joint, the mechanical properties of the matrix material are decisive in carrying the bending impact load. The shear damage occurring in the matrix region together with the impact load caused the contact force values to be realized at low levels.

## 3.2 Effect of Fiber Orientation Angle

The effect of fiber orientation angles for each impact angle on the contact force–time curve of the joint is shown in Fig. 7. Under normal impact load ($\theta = 0°$), the contact force
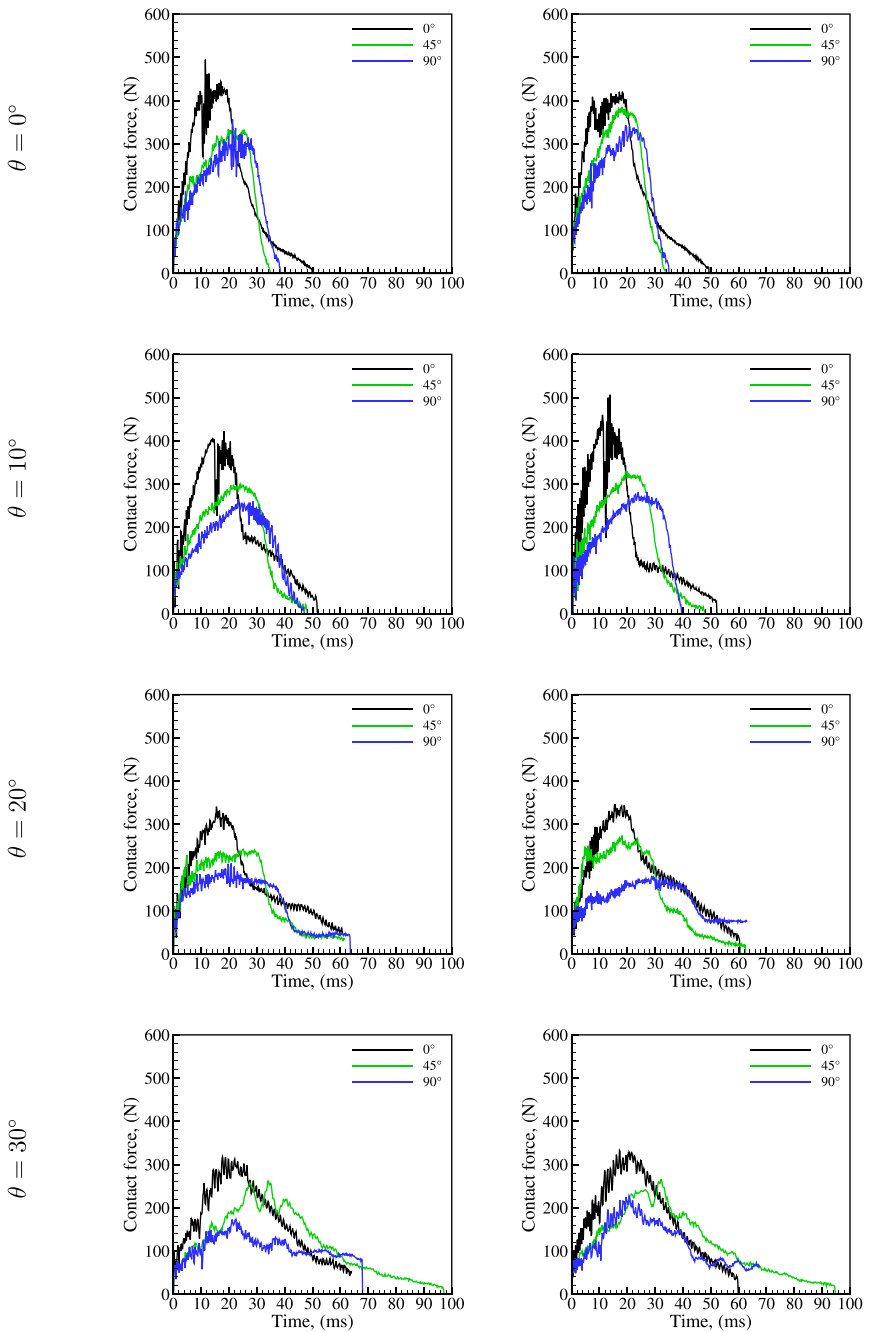
**Fig. 7** Contact force–time variations of composite single-lap joints having different fiber angles for different impact angles (*b*: overlap length, *θ*: impact angle)

reached its highest value in the single-lap joint with 0° fiber angle and decreased with the increase of the impact angle. Similarly, the contact time was longer for 0° fiber angle compared to the joints with other fiber angles. As the impact angle increased, the total contact time for 0° fiber angle increased approximately 10 ms, while the increase in the contact time for 45° and 90° fiber angles reached about 35–65 ms. The fiber angle of the adherends also determines the load carrying capacity of the joints. The joint with 0° fiber angle has the highest load carrying capacity whilst the joint with 90° fiber angle has the lowest load carrying capacity. It was observed from the impact tests that the joint with a low load carrying capacity was more sensitive to the increase in the impact angle.
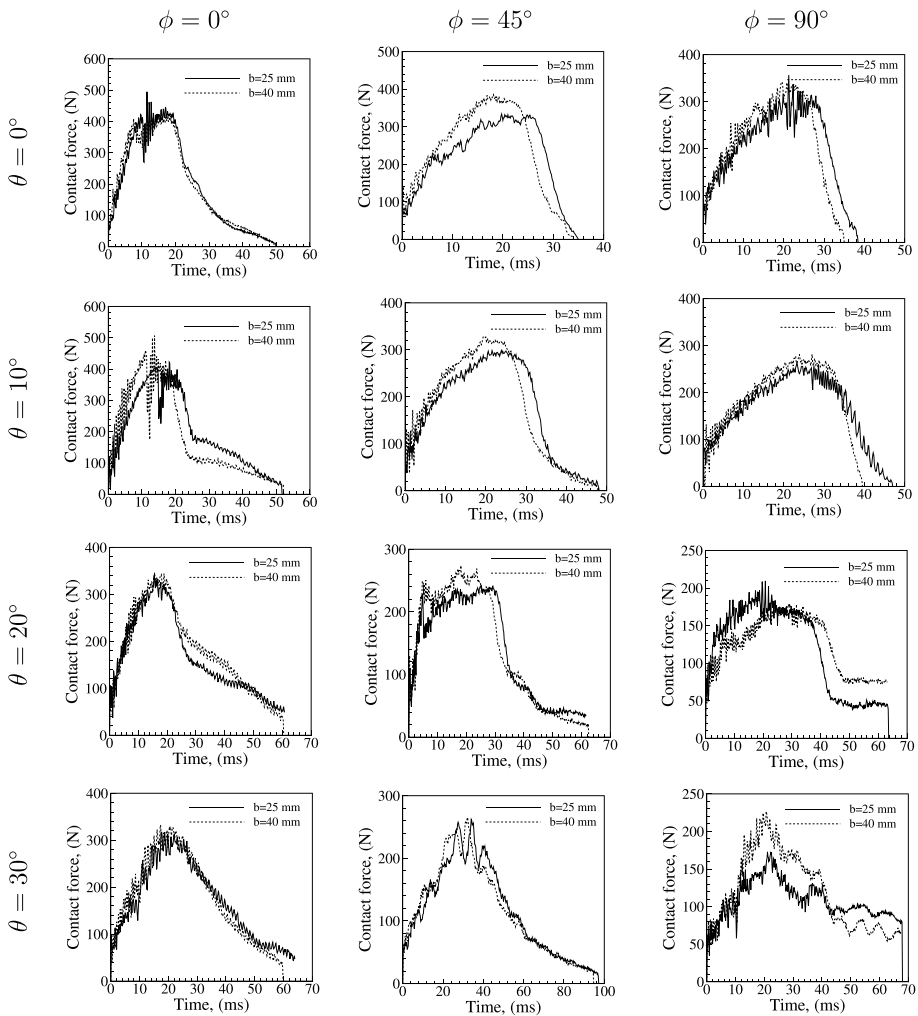


**Fig. 8** Contact force–time variations of composite single-lap joints with different overlap lengths (*b*: overlap length, *ϕ*: fiber angle, *θ*: impact angle)

### 3.3 Effect of Overlap Length

The effect of overlap length on contact force–time variations is shown in Fig. 8. As the bonding area increases with the increase in overlap length, the load carrying capacity of the joint also increases. For $E = 3.2$ J impact energy, the contact force–time variations were quite similar in the single-lap joints with overlap lengths of 25 and 40 mm. The similarity in these changes decreased with the increase in the amount of damage in the composite adherends. In the joint with the highest load carrying capacity (0° fiber angle), while the contact force–time variations in both overlap lengths were quite close to each other, the proximity between these variations decreased slightly in the joint with the lowest load carrying capacity (90° fiber angle). The maximum contact force slightly increased with increasing overlap length. Similar results were obtained by the researchers under both in-plane and out-of-plane impact loads [21, 26]. Since the increase in overlap length increases the strength and stiffness of the adhesive joints, the maximum contact force value and failure load of the joint is expected to increase under in-plane and out-of-plane impact loads. Matrix shear damage was observed apparently in the composite adherends with 90° fiber angle. A longer overlap length can improve bending stiffness. Although there was a negligible increase in contact force levels, not all of the applied impact energy could be dissipated by the joint with 90° fiber angle. Adhesively bonded joints are expected to maintain their structural integrity under impact load. The joints with 90° fiber angle were damaged at free edges by matrix shear damage for all impact angles under 3.2 J impact energy. For this reason, joints with 90° fiber angle were insufficient to meet the applied impact energy due to loss of structural integrity.

### 3.4 Contact Force–displacement Variation

The contact force–displacement variation of the joints under impact load is presented in Fig. 9. The vertical displacement value supplies information about the bending stiffness of the joints as well as the elastic energy storage of the joints under impact load. In addition, fluctuations in the contact force give information about the amount of damage that occurs in the joints. For joints with 0° fiber angle, the vertical displacement value increased up to the maximum contact force level, and after this point, the displacement value tended to decrease because it released the elastic energy stored. The elastic energy released by the joints in the rebound phase decreased as the impact angle increased. Adhesive damage was observed to be intense in the joints with 0° fiber angle. Therefore, significant fluctuations occurred in the contact force. The elastic energy storage capability of the joints was low, as significant damage occurs in the composite adherends in the joints with 45° and 90° fiber angles. Since the composite adherends and adhesive underwent damage in the joints with 45° fiber angle, the fluctuation amplitude in the contact force was higher. Matrix shear damage was more dominant in the composite adherends for the joints with 90° fiber angle. For this reason, the fluctuations in the contact force histories occurred intensively for joints with 90° fiber angle. The increase in the impact angle caused an increase in the vertical displacement value in the joints for all joint configurations. For a range of impact angle from 0° to 30°, the increase in the maximum vertical displacement value for joints with 25 mm overlap length was approximately 83, 53, and 116% for joints with 0°, 45°, and 90° fiber angle, respectively. In addition, for 40 mm overlap length, there was an increase of 62, 70, and 88% for joints with 0°, 45°, and 90° fiber angle, respectively.

Fiber angle                    $b = 25$ mm                           $b = 40$ mm
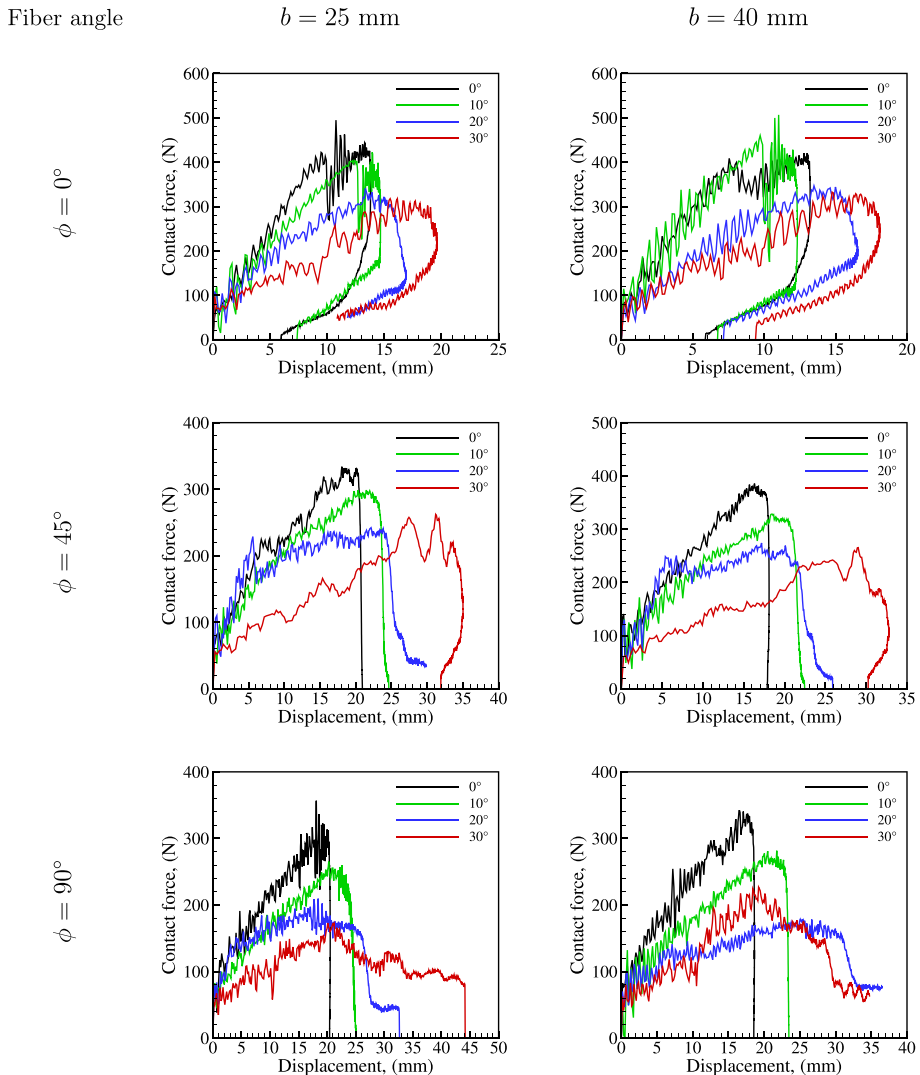


**Fig. 9** Contact force–displacement variations of composite single-lap joints for different impact angles ($b$: overlap length, $\phi$: fiber angle)

As seen, the impact and fiber angle have a significant effect on contact force level, total contact time, and peak displacement. In the joint with 0° fiber angle, the orientation of fibers carries the applied impact load effectively. In the joints with 45° and 90° fiber angles, the load carrying capacity of fibers gradually decreases and the applied impact load is carried by the matrix material. As a result of the shear stress increasing through the thickness of the composite adherend, the matrix material was damaged, and delamination damage also occurred along the fiber-matrix interfaces. The damage in the composite adherends caused the maximum contact force to decrease and the total contact time to increase. The impact load was sustained by both fibers and adhesive layer in the 0° fiber angle joint, by the fiber, matrix, and adhesive layer in the joint with 45° fiber angle, and by both matrix

and adhesive in the joint with 90° fiber angle. The impact load in the joint with 45° fiber angle caused evident shear stresses along the fiber-matrix interface in the composite adherends. The unbalanced in-plane shear stress distribution forced the joint to rotate in the longitudinal direction, and caused matrix and adhesive damages. The damage in the composite adherends significantly reduced the maximum contact force level.

## 4 Damage Analysis

Damage mechanism and damaged regions in the joints were evaluated in accordance with the ASTM D5573-99 Standard Practice for Classifying Failure Modes in Fiber-Reinforced-Plastic (FRP) Joints [51]. After the impact tests, macro and micro photographs of the damage regions were taken for the examination of the damage types in the overlap region. In the joints with adhesive damage, the boundaries of damaged adhesive regions were marked by inspection after the joint was completely separated by hand. When the failure surfaces of top and bottom composite adherend were examined, some amount of adhesive mostly accumulated on the bottom composite adherend surface, while a small amount of adhesive layer and broken fibers on the top composite adherend surface. In the detailed examination of damage morphology in composite joints, for this reason, the top composite adherend surfaces were only taken into consideration. First, the top photograph of the damage region was taken with the macroscope. Then, the magnified microscope images were obtained in three regions of the damaged surface. These regions can be classified as the damage initiation, propagation and ending regions. Thus, different damage types occurred in both adhesive layer and composite materials. Microscope images were obtained with the ZEISS Axio Imager 2 device since the surface of many materials such as metallic, composite, and wood can be examined in detail with this device. The microscope images of damaged composite surfaces were obtained in the dark-field mode.
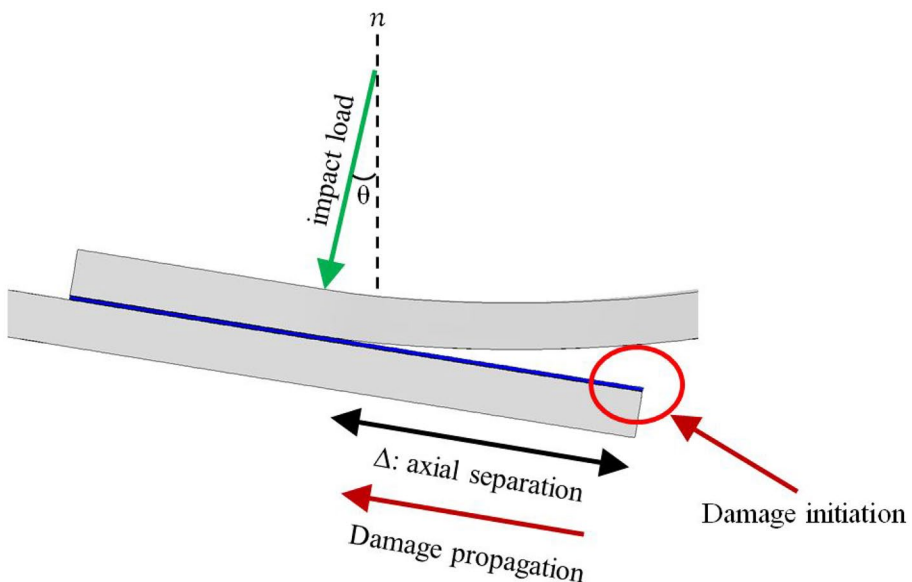


**Fig. 10** Schematic representation of adhesive damage propagation in the joint under impact load

## 4.1 Adhesive Damage Initiation and Propagation

The adhesive damage initiation and propagation under impact load are shown sche-matically in Fig. 10. Adhesive damage initiated from the right free edge and propagated through the overlap region. The axial separation length (Δ) was determined by considering where the adhesive damage initiated and ended. Under normal impact load, the initiation and propagation of adhesive damage occurred with the effect of peak peel stress in the free edges of damaged overlap region. However, under oblique impact, the impact load has two force components. The force normal to the joint caused adhesive damage due to its peeling effect, while the tangential force component parallel to the joint caused adhesive damage with a shear effect. The force components of the impact load which cause shear and peel-ing effect in adhesive layer depend on the impact angle. As the impact angle increases, the tangential force component increases while the normal force component decreases. The axial separation lengths of composite single-lap joints for different impact angles are pre-sented in Fig. 11. The maximum axial separation length appeared in the joints having the highest bending strength with 0° fiber angle. Both adhesive and adherend undergo damage. Since the weakest part is adhesive layer in the joint with the highest bending strength, the adhesive damage is immense. The minimum axial separation occurred in the joints hav-ing the lowest bending strength with 90° fiber angle. In the joints with 90° fiber angle, the impact energy was absorbed only both matrix and adhesive. Matrix shear damage, rather than adhesive damage, was observed in these joints due to higher shear stresses at the free edges of the overlap region. The axial separation length (Δ) also decreased with increasing impact angle. Therefore, this indicates that the resistance of adhesive against shear stress was higher than those against the peeling stress.

## 4.2 Detailed Damage Examination with Microscope Image

The microscope images of fracture of adherends surfaces are shown in Fig. 12. Microscope images were taken along the top composite-adhesive interface. The microscope images taken from the damaged surface of the joint with 0° fiber angle and 25 mm overlap length under normal impact are shown in Fig. 13. The amount of adhesive residues on the sur-face was denser in the selected regions (A, B, C) in the damage initiation zone. Delamina-tion damage occurred in the top composite material around the adhesive, resulting in the emergence of fibers. The microscope images indicated that the peeling effect occurring in the initiation region of damage under bending impact load caused the fibers to rupture. In regions where the damage progressed (D, E, F), mostly delamination and fiber-tear damage occurred. In the damage-ending zone, a large amount of adhesive residues was seen on the fracture surfaces. This implies that the damage in the joint initiated in the adhesive, then progressed at the upper composite-adhesive interface and penetrated in to the composite, thus causing fiber breakages and progressing into the adhesive layer towards the end zone. In the joints, adhesive and epoxy are two materials, whose mechanical properties are rela-tively weak compared to fibers. The damage initiated from the weak region in the joint sub-jected to peeling effects and even caused fiber-tear due to the impact energy.

The microscope photographs of the damage surfaces of the joint with 40 mm overlap length are shown in Fig. 13. In the joint, since the bending stiffness increased with increas-ing overlap length, delamination and fiber-tear damage were also observed. The increase in bending stiffness caused the damage to initiate in vicinity of the interface between the
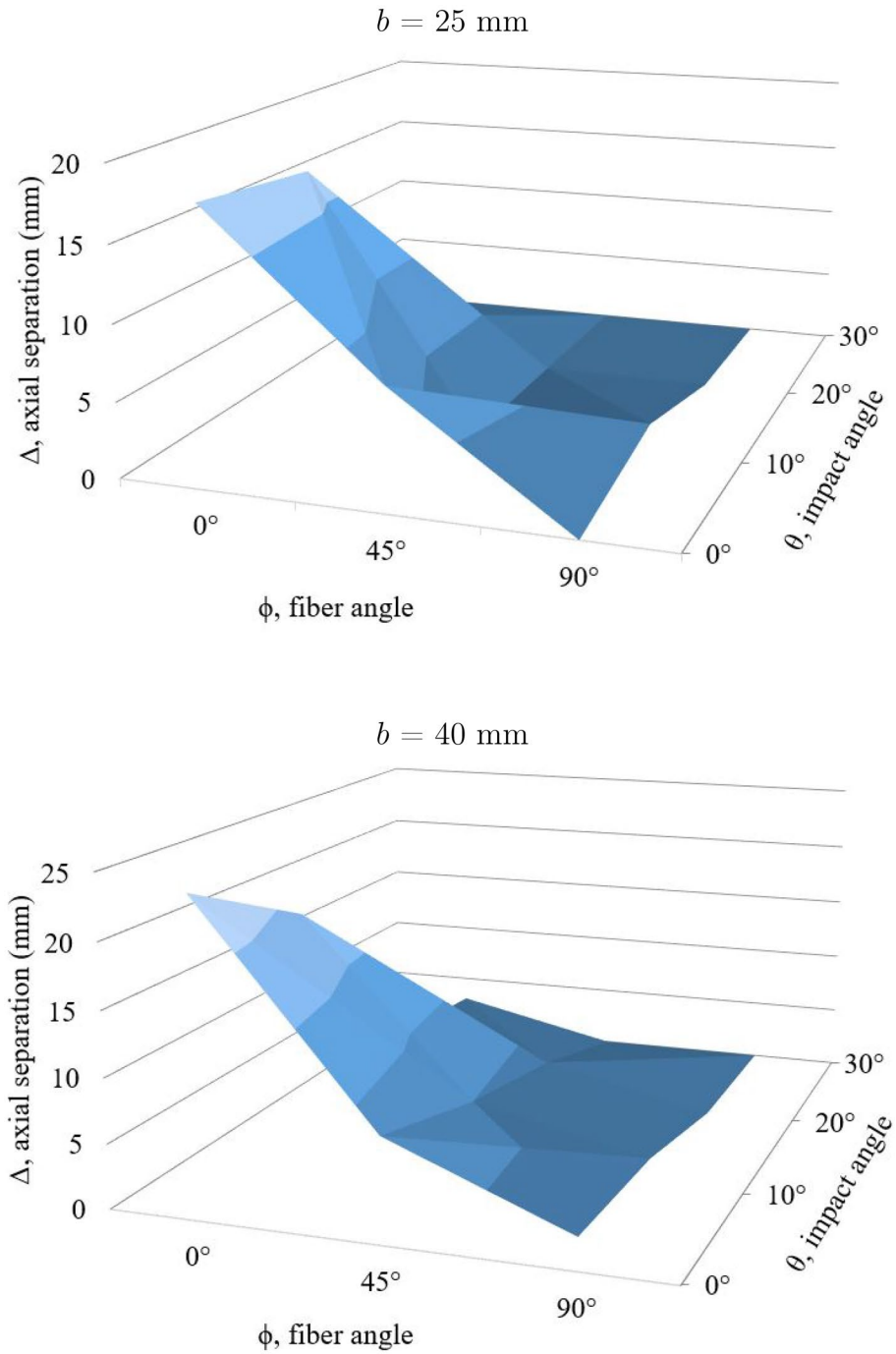
**Fig. 11** Effects of fiber angle and impact angle on axial separation of composite single-lap joints (*b*: overlap length)

**Fig. 12** Schematic representation of microscope images of the fracture surfaces of joints (Figs. 13, 14, and 15)

composite and adhesive instead of through the adhesive layer. In the damage propagation region, the fibers due to delamination emerged. Fiber-tear damage also occurred in these regions. Adhesive residues appeared in the damage-ending zone. The damage towards the damage-ending zone was progressed mostly inside the adhesive. Namely, the adhesive residues on the damaged surface of the top composite adherend significantly reduced.

The effect of impact angle on the damage initiation and propagation is visualized with the photographs of damaged surfaces in Fig. 14. The increase in the impact angle caused the initiation of damage to be largely developed in the adhesive layer. The damage in the adhesive material due to shear stress also increased with increasing impact angle. Fiber-tear damage decreased with increasing impact angle. The effect of peeling stresses is apparent on fiber-tear damage. The damage initiated in the adhesive layer, and spread along the adhesive region close to the top composite-adhesive interface.

The joint with 45° fiber angle cannot carry the load evenly in the adherend plane, so the joint is forced to rotate about its longitudinal axis. The effect of this unbalanced in-plane shear force distribution on the damage is shown in Fig. 15. The joint was usually damaged in the 45° fiber direction. The moment due to the unbalanced in-plane shear force distribution also contributed to the state of shear stress in the overlap region. In case the microscope images of damaged surfaces were examined, the damage occurred within the adhesive layer and propagated along the top composite and adhesive interface. The broken fibers are clearly seen in the micro-photographs of damage surfaces. The matrix (epoxy) also underwent significant damage as a result of higher shear stress distribution in the overlap region. The increased shear stresses in the joint with 45° fiber angle (unbalanced joint) were evident in the adhesive and epoxy matrix. However, the effect of the increase in shear stress levels is of a negligible effect on fiber-tear damage. The damage mechanism of adhesively bonded joints under transverse low-speed impact has been investigated in some studies in the open literature [14, 26, 28, 33, 50]. He and Pan [28] reported that the predominant damage type was matrix shear damage and adhesive damage initiated from the free edge and propagated through the overlap region. Liu and Yan [33] stated that adhesive damage, matrix shear damage, and delamination occurred together in joints due to the transverse impact load. In general, it was attempted to determine the relationship between peel and shear stress distributions in the overlap region and adhesive damage
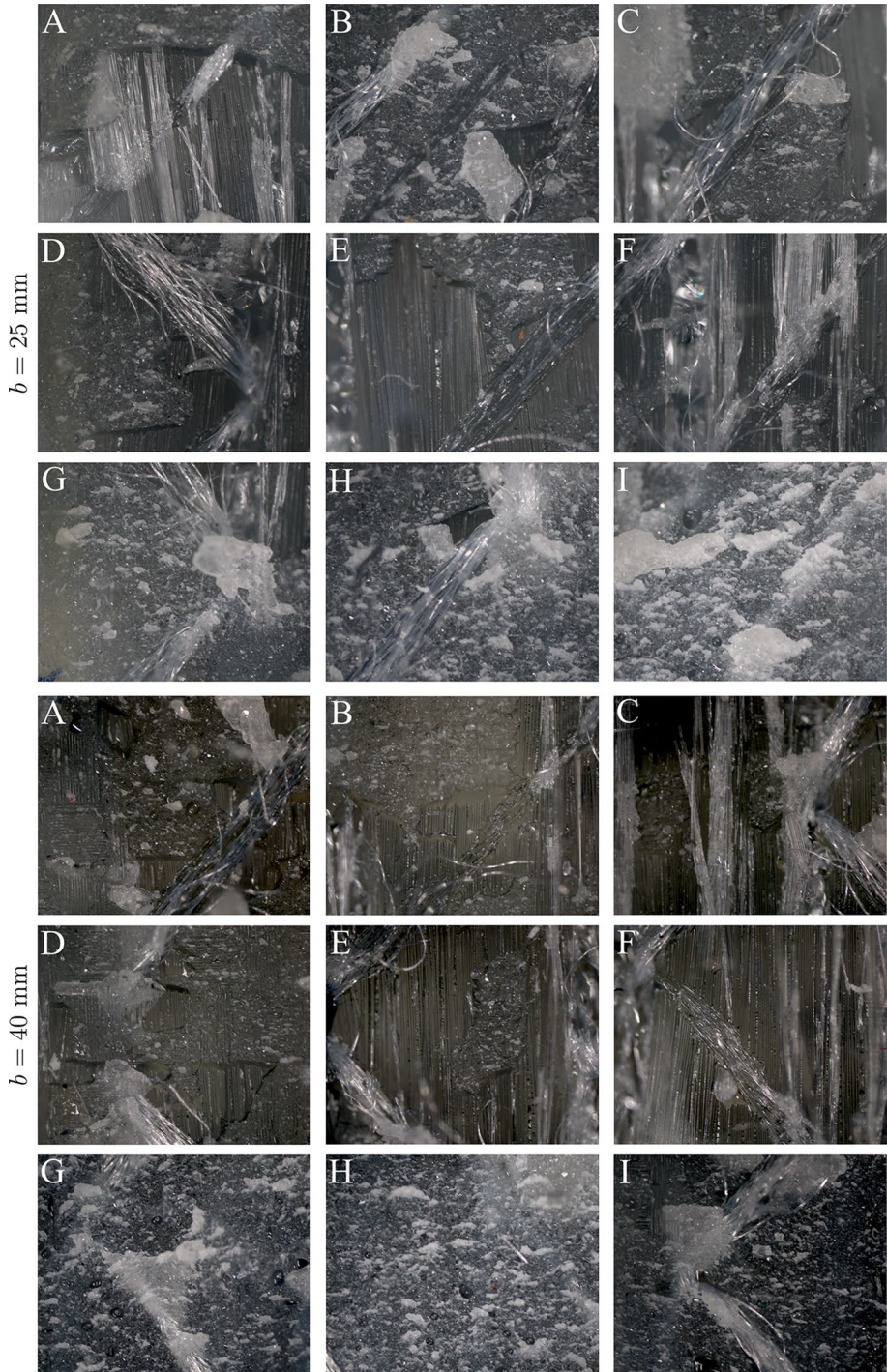
**Fig. 13** Microscope images of the damaged top composite-adhesive interface of the joint with 0° fiber angle and 0° impact angle (*b*: overlap length)
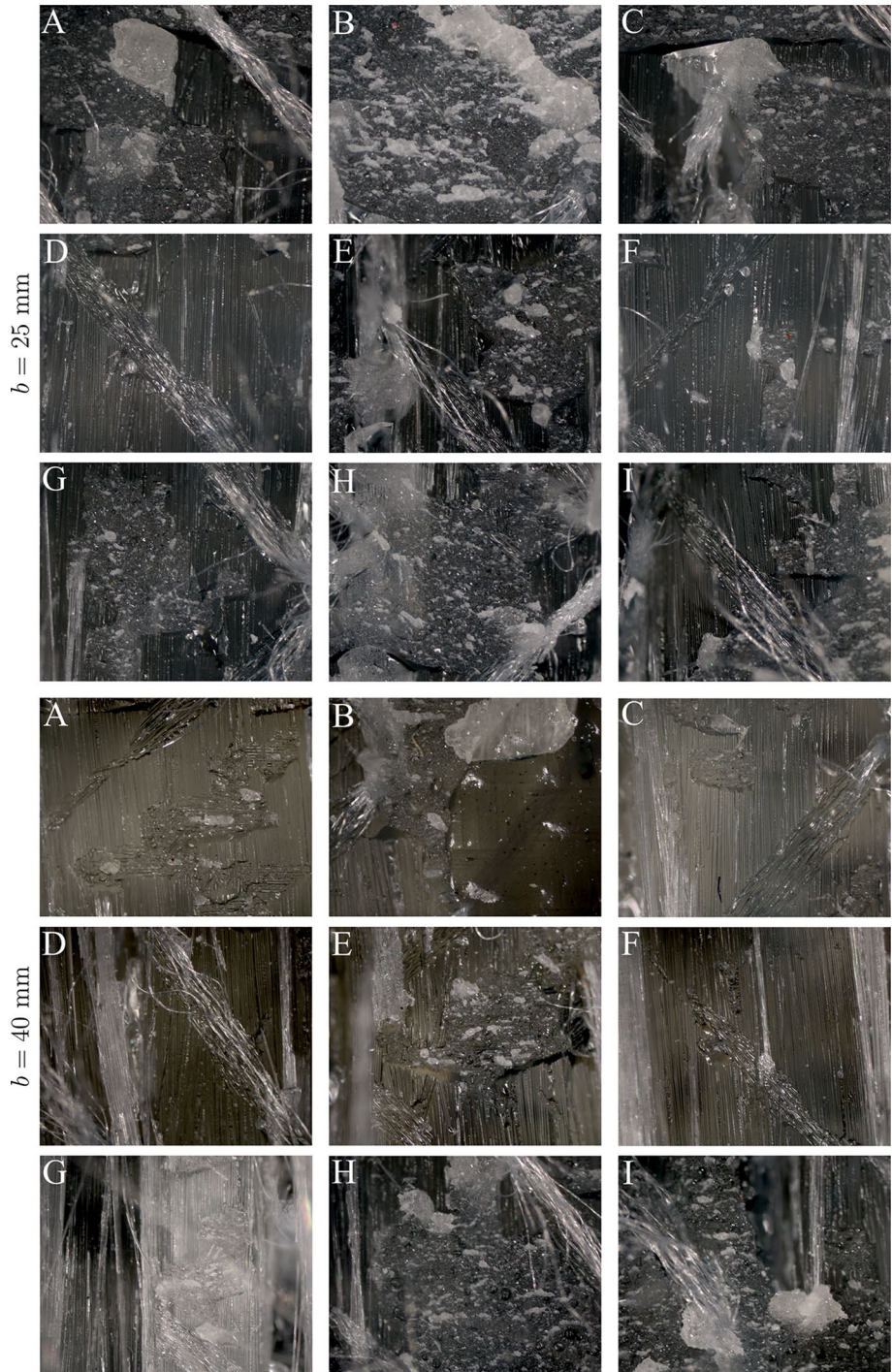
**Fig. 14** Microscope images of the damaged top composite-adhesive interface of the joint with 0° fiber angle and 10° impact angle (*b*: overlap length)
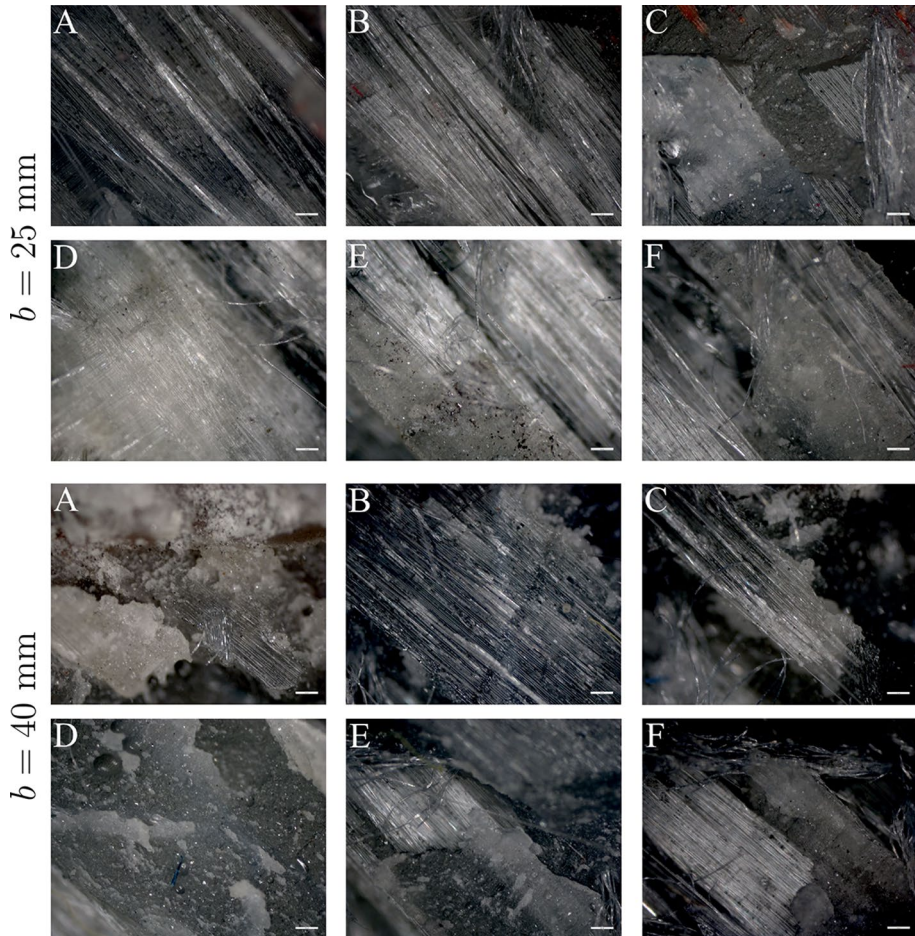
**Fig. 15** Microscope images of the damaged top composite-adhesive interface of the joint with 45° fiber angle and 0° impact angle (*b*: overlap length)

initiation and propagation [14, 26, 28, 50]. It was shown that the peeling and shear stresses were concentrated at the free edges of the overlap region under the transverse impact load; therefore, the adhesive damage initiated at the free edges of the overlap region. This study indicates damage types, initiation and propagation mechanisms similar to those in the open literature. Due to the bending impact load, in-plane tensile, compressive axial stresses and shear stresses, and out-of-plane shear stresses occurred. Both in-plane and out-of-plane shear stresses caused matrix shear damage in the joints with 45° fiber angle whilst the axial stress through the thickness of adherends resulted in fiber breakage especially in vicinity of the top composite-adhesive interface. However, the out-of-plane shear stresses were more effective in matrix shear damage in the joints with 90° fiber angle. Both peeling and in-plane shear stresses caused adhesive damage in the joints with 0° fiber angle. Therefore, the composite failure mechanism was formed by the effect of in-plane and out-of-plane stresses, while the adhesive damage mechanism depends on both peeling and shear stresses.

# 5 Conclusions

In this study, the effects of impact angle, fiber angle and overlap length on the mechanical behavior and damage formation of composite single-lap joints under low velocity oblique impact load were experimentally investigated. The normal and tangential components of oblique impact load are obviously varied with an increase in the oblique impact angle. The in-plane fiber angle of both composite adherends changes the bending strength of joints. The joint with 0° fiber angle has the highest bending strength, while the joint with 90° fiber angle has the lowest bending strength. The joint with 45° fiber angle is unbalanced and the effect of unbalanced in-plane shear stress distributions on the impact behavior was apparent. A longer overlap length increases the flexural strength of joints and the increased adhesive amount can be capable of absorbing most of the impact energy. Based on the experimental results the following conclusions are made:

- The decrease in the maximum contact force with increasing impact angle was the lowest in the 0° fiber angle joint with the highest bending strength compared to the other joint types. The highest decrease in the maximum contact force was observed in the joint with the lowest flexural strength of 90° fiber angle. The joint with low bending strength was more sensitive to increasing impact angle.
- As the fiber angle is increased, the bending stiffness of joints considerably decreases. Therefore, the matrix is forced to experience most of the bending impact energy. In the composite joint with 0° fiber angle, the bending load was met by both fiber and adhesive, and in the 90° fiber angle joint by matrix and adhesive.
- The increase in the flexural strength of joints also increased the maximum contact force level. The impact energy caused significant damage in the composite adherends of the joints with 45° and 90° fiber angles. Therefore, the vertical displacements were larger than those in the joints with 0° fiber angle. The measured maximum vertical displacements were affected by both impact angle and fiber angle.
- As the impact energy was absorbed mostly by both adhesive damage and elastic deformation in the 0° fiber angle joints with the highest bending strength, it was absorbed by the damages in both composite adherend and adhesive and elastic deformation on the joints with 45° and 90° fiber angles. The intension of damage in the composite adherends gets higher.

# 6 Future Research Direction

In addition to the experimental study on the impact behavior and damage mechanism of adhesively bonded joints, a numerical investigation can allow us to trace the damage formation and propagation during the impact duration in incremental sense. Low speed impact analysis of adhesively bonded composite joint requires the consideration of complicated material constitutive relations, contact conditions, etc. However, the reasonable numerical analysis of adhesively bonded composite joints provides incremental damage propagation, which is difficult experimentally and to examine the effect of various design parameters on the low speed impact response of adhesively bonded composite single-lap joints as well as on their damage mechanisms.

# References

1. Da Silva, L.F., Öchsner, A., Adams, R.D.: Handbook of Adhesion Technology, p. 1554. Verlag Berlin Heidelberg, Springer Science & Business Media (2011)
2. Adams, R.D., Comyn, J., Wake, W.C.: Structural Adhesive Joints in Engineering, p. 359. Chapman & Hall, London (1997)
3. da Silva, L.F.M., Pirondi, A., Öchsner, A.: Hybrid Adhesive Joints, p. 309. Springer Science & Business Media, Berlin, Heidelberg (2011)
4. Machado, J.J.M., Marques, E.A.S., da Silva, L.F.M.: Adhesives and adhesive joints under impact loadings: An overview. J. Adhes. **94**(6), 421–452 (2018)
5. Harris, J., Adams, R.: An assessment of the impact performance of bonded joints for use in high energy absorbing structures. Proc. Inst. Mech. Eng. C. J. Mech. Eng. Sci. **199**(2), 121–131 (1985)
6. Srivastava, V., Shukla, A., Parameswaran, V.: Experimental evaluation of the dynamic shear strength of adhesive-bonded lap joints. J. Test. Eval. **28**(6), 438–442 (2000)
7. Yokoyama, T.: Experimental determination of impact tensile properties of adhesive butt joints with the split hopkinson bar. J. Strain. Anal. Eng. Des. **38**(3), 233–245 (2003)
8. Sato, C., Iwata, H., Ikegami, K.: Dynamic deformation of tapered lap adhesive joint under impact loading. JSME. Int. J. Ser. A. Mech. Mater. Eng. **40**(1), 31–36 (1997)
9. Sawa, T., Suzuki, Y., Kido, S.: Fem stress analysis and strength of adhesive butt joints of similar hollow cylinders under static and impact tensile loadings. J. Adhes. Sci. Technol. **16**(11), 1449–1468 (2002)
10. Higuchi, I., Sawa, T., Suga, H.: Three-dimensional finite element analysis of single-lap adhesive joints under impact loads. J. Adhes. Sci. Technol. **16**(12), 1585–1601 (2002)
11. Higuchi, I., Sawa, T., Suga, H.: Three-dimensional finite element analysis of single-lap adhesive joints subjected to impact bending moments. J. Adhes. Sci. Technol. **16**(10), 1327–1342 (2002)
12. Sawa, T., Higuchi, I., Suga, H.: Three-dimensional finite element stress analysis of single-lap adhesive joints of dissimilar adherends subjected to impact tensile loads. J. Adhes. Sci. Technol. **17**(16), 2157–2174 (2003)
13. Sato, C., Ikegami, K.: Dynamic deformation of lap joints and scarf joints under impact loads. Int. J. Adhes. Adhes. **20**(1), 17–25 (2000)
14. Asgharifar, M., Kong, F., Carlson, B., Kovacevic, R.: Dynamic analysis of adhesively bonded joint under solid projectile impact. Int. J. Adhes. Adhes. **50**, 17–31 (2014)
15. Banea, M.D., da Silva, L.F.M., Campilho, R.D.S.G., Sato, C.: Smart adhesive joints: An overview of recent developments. J. Adhes. **90**(1), 16–40 (2014)
16. You, M., Li, M.-B., Yuan, Y.-L., Lin, G., Ma, F.-W., Du, L.-F., Tang, S.-J.: Review of experimental techniques for impact property of adhesive bonds. Int. J. Adhes. Adhes. **100**, 102620 (2020)
17. Chen, C., Sun, C., Han, X., Hu, D., Zhou, J., Guan, Z.: The structural response of the thermoplastic composite joint subjected to out-of-plane loading. Int. J. Impact. Eng. **145**, 103691 (2020)
18. Bautista, A., Casas-Rodriguez, J., Silva, M., Porras, A.: A dynamic response analysis of adhesive-bonded single lap joints used in military aircrafts made of glass fiber composite material undercyclic impact loading. Int. J. Adhes. Adhes. **102**, 102644 (2020)
19. Araújo, H., Machado, J., Marques, E., Da Silva, L.: Dynamic behaviour of composite adhesive joints for the automotive industry. Compos. Struct. **171**, 549–561 (2017)
20. Hou, W., Xu, X., Sang, L., Tong, L.: Failure of single hat-shaped thin-walled tubular composite t-joints under impact loading. Thin-Walled Struct. **154**, 106815 (2020)
21. Machado, J., Marques, E., Da Silva, L.: Mechanical behaviour of adhesively bonded composite single lap joints under quasi-static and impact conditions with variation of temperature and overlap. J. Compos. Mater. **52**(26), 3621–3635 (2018)
22. Basri, A.B.A., Chae, D.W., Lee, H.: Investigation of the dynamic characteristics of a carbon-fiber-reinforced epoxy with adhesive-jointed structure. Compos. Struct. **247**, 112499 (2020)
23. Yildirim, M., Apalak, M.K.: Transverse low-speed impact behavior of adhesively bonded similar and dissimilar clamped plates. J. Adhes. Sci. Technol. **25**(1–3), 69–91 (2011)

24. Apalak, M.K., Yildirim, M.: Effect of adhesive thickness on transverse low-speed impact behavior of adhesively bonded similar and dissimilar clamped plates. J. Adhes. Sci. Technol. **25**(19), 2587–2613 (2011)
25. Hülagü, B., Ünal, H.Y., Acar, V., Khan, T., Aydın, M.R., Aydın, O.A., Gök, S., Pekbey, Y., Akbulut, H.: Low-velocity impact and bending response of graphene nanoparticlereinforced adhesively bonded double strap joints. J. Adhes. Sci. Technol. **35**(22), 2391–2409 (2021)
26. Hu, C., Huang, G., Li, C.: Experimental and numerical study of low-velocity impact and tensile after impact for cfrp laminates single-lap joints adhesively bonded structure. Materials. **14**(4), 1016 (2021)
27. Kaybal, H.B., Ulus, H., Eskizeybek, V., Avcı, A.: An experimental study on low velocity impact performance of bolted composite joints part 1: Influence of halloysite nanotubes on dynamic loading response. Compos Struct. **258**, 113415 (2021)
28. He, B., Pan, Y.: Failure mechanism of single lap adhesively bonded composite-titanium joints subjected to solid projectile impact. J. Adhes. Sci. Technol. (2021)
29. Li, J., Li, Y., Xiang, Y., Chen, J.: Effect of low-velocity impact on the strength and durability of bonded joint in hygrothermal environment. J. Adhes. (2021)
30. Kadioglu, F., Adams, R.D.: Flexible adhesives for automotive application under impact loading. Int. J. Adhes. Adhes. **56**, 73–78 (2015)
31. Hazimeh, R., Othman, R., Khalil, K., Challita, G.: Influence of plies' orientations on the stress distribution in adhesively bonded laminate composite joints subjected to impact loadings. Compos. Struct. **152**, 654–664 (2016)
32. Atahan, M.G., Apalak, M.K.: Low-speed bending impact behavior of adhesively bonded single-lap joints. J. Adhes. Sci. Technol. **31**(14), 1545–1575 (2017)
33. Liu, B., Yan, R.: Damage mechanism and residual strength at different impact locations for composite bonding scarf repairs. J. Adhes. Sci. Technol. **32**(23), 2523–2536 (2018)
34. Huang, W., Sun, L., Li, L., Shen, L., Huang, B., Zhang, Y.: Investigations on low-energy impact and post-impact fatigue of adhesively bonded single-lap joints using composites substrates. J. Adhes. **96**(15), 1326–1354 (2020)
35. Silva, N., Machado, J., Marques, E., Moreira, P., da Silva, L.: Experimental and numerical study of the dynamic response of an adhesively bonded automotive structure. Proc. Inst. Mech. Eng. D. J. Automob. Eng. **234**(14), 3385–3397 (2020)
36. Li, Y., Yang, Y., Li, J., Wang, B., Liao, Y.: Experimental-numerical analysis of failure of adhesively bonded lap joints under transverse impact and different temperatures. Int. J. Impact. Eng. **140**, 103541 (2020)
37. Machado, J., Nunes, P., Marques, E., da Silva, L.F.: Adhesive joints using aluminium and cfrp substrates tested at low and high temperatures under quasi-static and impact conditions for the automotive industry. Compos. B. Eng. **158**, 102–116 (2019)
38. Avendaño, R., Carbas, R., Chaves, F., Costa, M., Da Silva, L., Fernandes, A.: Impact loading of single lap joints of dissimilar lightweight adherends bonded with a crash-resistant epoxy adhesive. J. Eng. Mater. Technol. **138**(4), 041019 (2016)
39. Song, J.: Numerical simulation on windowed tubes subjected to oblique impact loading and a new method for the design of obliquely loaded tubes. Int. J. Impact. Eng. **54**, 192–205 (2013)
40. Ivañez, I., Moure, M., Garcia-Castillo, S., Sanchez-Saez, S.: The oblique impact response of composite sandwich plates. Compos. Struct. **133**, 1127–1136 (2015)
41. Purimpat, S., Jérôme, R., Shahram, A.: Effect of fiber angle orientation on a laminated composite single-lap adhesive joint. Adv. Compos. Mater. **22**(3), 139–149 (2013)
42. ASTM International. ASTM D3039 / D3039M - 17, Standard Test Method for Tensile Properties of Polymer Matrix Composite Materials. https://www.astm.org/d3039_d3039m-08.html
43. ASTM International. ASTM D3410 - 87, Standart Test Method for Compressive Properties of Unidirection or Cross-ply Fiber-resin Composite. https://www.astm.org/Standards/D3410
44. ASTM International. ASTM D7078 / D7078M - 19, Standard Test Method for Shear Properties of Composite Materials by V-Notched Rail Shear Method. https://www.astm.org/d7078_d7078m-05.html
45. Kaddour, A., Hinton, M.J., Smith, P.A., Li, S.: Mechanical properties and details of composite laminates for the test cases used in the third world-wide failure exercise. J. Compos. Mater. **47**(20–21), 2427–2442 (2013)
46. Aktaş, M., Karakuzu, R.: Determination of mechanical properties of glass-epoxy composites in high temperatures. Polym. Compos. **30**(10), 1437–1441 (2009)
47. Icten, B.M., Atas, C., Aktas, M., Karakuzu, R.: Low temperature effect on impact response of quasi-isotropic glass/epoxy laminated plates. Compos. Struct. **91**(3), 318–323 (2009)
48. Lapczyk, I., Hurtado, J.A.: Progressive damage modeling in fiber-reinforced materials. Compos. A. Appl. Sci. Manuf. **38**(11), 2333–2341 (2007)

49. Huntsman Corporation. Araldite 2015 epoxy adhesive, Huntsman Advanced Materials. http://www.huntsman.com
50. Vaidya, U.K., Gautam, A.R., Hosur, M., Dutta, P.: Experimental–numerical studies of transverse impact response of adhesively bonded lap joints in composite structures. Int. J. Adhes. Adhes. **26**(3), 184–198 (2006)
51. ASTM International. ASTM D5573 - 99, Standard Practice for Classifying Failure Modes in Fiber-Reinforced-Plastic (FRP) Joints (2019). https://www.astm.org/d5573-99r19.html

**Publisher's Note**  Springer Nature remains neutral with regard to jurisdictional claims in published maps and institutional affiliations.